

# Search for reactor-produced millicharged particles with Skipper-CCDs at the CONNIE and Atucha-II experiments

Alexis A. Aguilar-Arevalo, Juan Carlos D'Oliveo, and Youssef Sarkis

*Instituto de Ciencias Nucleares, Universidad Nacional Autónoma de México, Circuito Exterior s/n, C.U., CDMX, Mexico*

Nicolas Avalos and Xavier Bertou

*Centro Atómico Bariloche and Instituto Balseiro,  
Comisión Nacional de Energía Atómica (CNEA),*

*Consejo Nacional de Investigaciones Científicas y Técnicas (CONICET),  
Universidad Nacional de Cuyo (UNCUYO), Av Bustillo 9500, San Carlos de Bariloche, Argentina*

Pablo Bellino

*Comisión Nacional de Energía Atómica, Centro Atómico Constituyentes*

Carla Bonifazi

*International Center for Advanced Studies & Instituto de Ciencias Físicas,  
ECyT-UNSAM and CONICET, 25 de Mayo y Francia, Buenos Aires, Argentina and  
Instituto de Física, Universidade Federal do Rio de Janeiro,  
Av. Athos da Silveira Ramos, 149, Cidade Universitária, Rio de Janeiro, RJ, Brazil*

Ana Botti, Gustavo Cancelo, Juan Estrada, Richard Ford, Kevin Kuk, Andrew Lathrop, and Javier Tiffenberg

*Fermi National Accelerator Laboratory, Batavia, IL, United States*

Mariano Cababié

*Institut für Hochenergiephysik der Österreichischen Akademie der Wissenschaften, 1050 Wien - Austria and  
Atominstytut, Technische Universität Wien, 1020 Wien - Austria*

Brenda A. Cervantes-Vergara

*Instituto de Ciencias Nucleares, Universidad Nacional Autónoma de México,  
Circuito Exterior s/n, C.U., CDMX, Mexico and  
Fermi National Accelerator Laboratory, Batavia, IL, United States*

Claudio Chavez

*Fermi National Accelerator Laboratory, Batavia, IL, United States  
Instituto de Inv. en Ing. Eléctrica “Alfredo Desages” (IIIE),  
Dpto. de Ing. Eléctrica y de Computadoras, CONICET and Universidad Nacional del Sur (UNS),  
800 San Andrés Street, Bahía Blanca, Argentina and  
Facultad de Ingeniería, Universidad Nacional de Asunción, Campus de la UNA, San Lorenzo, Paraguay*

Fernando Chierchie

*Instituto de Inv. en Ing. Eléctrica “Alfredo Desages” (IIIE),  
Dpto. de Ing. Eléctrica y de Computadoras, CONICET and Universidad Nacional del Sur (UNS),  
800 San Andrés Street, Bahía Blanca, Argentina*

David Delgado

*Central Nuclear ATUCHA I-II, Nucleoeléctrica Argentina Sociedad Anónima, Buenos Aires, Argentina*

Eliana Depaoli

*Comisión Nacional de Energía Atómica, Centro Atómico Constituyentes and  
Universidad de Buenos Aires, Facultad de Ciencias Exactas y Naturales,  
Departamento de Física, Buenos Aires, Argentina*

João dos Anjos and Herman P. Lima Jr.

*Centro Brasileiro de Pesquisas Físicas, Rua Dr. Xavier Sigaud, 150, Urca, Rio de Janeiro, RJ, Brazil*

Guillermo Fernandez Moroni

*Fermi National Accelerator Laboratory, Batavia, IL, United States  
Instituto de Inv. en Ing. Eléctrica “Alfredo Desages” (IIIE),*

*Dpto. de Ing. Eléctrica y de Computadoras, CONICET and Universidad Nacional del Sur (UNS),  
800 San Andrés Street, Bahía Blanca, Argentina and  
Department of Astronomy and Astrophysics, University of Chicago,  
5640 South Ellis Avenue, Chicago, IL, 60637, USA*

*Aldo R. Fernandes Neto  
Centro Federal de Educação Tecnológica Celso Suckow da Fonseca,  
Campus Angra dos Reis, Rua do Areal, 522, Pq Mambucaba, Angra dos Reis, RJ, Brazil*

*Ben Kilminster  
Physik Institut, Universität Zürich, Winterthurerstrasse 190, Zurich, Switzerland*

*Patrick Lemos, Katherine Maslova, Irina Nasteva, Ana Carolina Oliveira, and Pedro Ventura  
Instituto de Física, Universidade Federal do Rio de Janeiro,  
Av. Athos da Silveira Ramos, 149, Cidade Universitária, Rio de Janeiro, RJ, Brazil*

*Martin Makler  
International Center for Advanced Studies & Instituto de Ciencias Físicas,  
ECyT-UNSAM and CONICET, 25 de Mayo y Francia, Buenos Aires, Argentina and  
Centro Brasileiro de Pesquisas Físicas, Rua Dr. Xavier Sigaud, 150, Urca, Rio de Janeiro, RJ, Brazil*

*Agustina Magnoni  
Departamento de Física, FCEN, Universidad de Buenos Aires, Buenos Aires, Argentina and  
Laboratorio de Óptica Cuántica, DEILAP, UNIDEF (CITEDEF-CONICET), Buenos Aires, Argentina*

*Franciole Marinho  
Departamento de Física, Instituto Tecnológico de Aeronáutica,  
DCTA, 12228-900, São José dos Campos, São Paulo, Brazil*

*Jorge Molina and Diego Stalder  
Facultad de Ingeniería, Universidad Nacional de Asunción, Campus de la UNA, San Lorenzo, Paraguay*

*Santiago Perez\* and Dario Rodrigues†  
Universidad de Buenos Aires, Facultad de Ciencias Exactas y Naturales,  
Departamento de Física. Buenos Aires, Argentina  
CONICET - Universidad de Buenos Aires, Instituto de Física de Buenos Aires (IFIBA). Buenos Aires, Argentina and  
Fermi National Accelerator Laboratory, Batavia, IL, United States*

*Laura Paulucci  
Universidade Federal do ABC, Avenida dos Estados 5001, Santo André, SP, Brazil*

*Ivan Sidelnik  
Departamento de Física de Neutrones, Centro Atómico Bariloche, (CNEA, CONICET), Bariloche, Argentina*

*Miguel Sofo Haro  
Universidad Nacional de Córdoba, CONICET (IFEG) and CNEA (RA0), Córdoba, Argentina  
(CONNIE and Atucha-II Collaborations)  
(Dated: May 28, 2024)*

Millicharged particles, proposed by various extensions of the standard model, can be created in pairs by high-energy photons within nuclear reactors and can interact electromagnetically with electrons in matter. Recently, the existence of a plasmon peak in the interaction cross-section with silicon in the eV range was highlighted as a promising approach to enhance low-energy sensitivities. The CONNIE and Atucha-II reactor neutrino experiments utilize Skipper-CCD sensors, which enable the detection of interactions in the eV range. We present world-leading limits on the charge of millicharged particles within a mass range spanning six orders of magnitude, derived through a comprehensive analysis and the combination of data from both experiments.

Short baseline reactor antineutrino experiments arise as an opportunity to look for beyond the standard model

(BSM) particles, such as QCD axions [1, 2], and other dark matter candidates [3–5]. Among the extensions to the standard model, millicharged particles (mCP) have gained significant attention and are considered highly compelling BSM candidates [6?, 7]. The TEXONO collaboration employed a point-contact 500 g germanium detector with a low-energy threshold of 300 eV, positioned 28 m away from a 2.9 GW<sub>th</sub> nuclear reactor, to set the most stringent direct laboratory exclusion limits below 1 MeV up to date [8].

Silicon detectors have pushed the energy thresholds to lower values, allowing for higher sensitivity in the dark-matter low-mass range. CONNIE [9, 10] was the first experiment to use silicon charge-coupled devices (CCD) at nuclear reactor to look for coherent elastic neutrino-nucleus scattering and impose competitive constraints on BSM physics [11]. Recently, CONNIE upgraded its detector by substituting the CCDs with a pair of Skipper-CCDs [12], increasing its sensitivity and low-energy reach [13]. At the same time, the Atucha-II experiment has deployed a Skipper-CCD sensor at nuclear power plant, situated just 12 m from the reactor core. Preliminary results exhibit a promising potential to explore both standard-model physics and exotic searches [14].

In a recent contribution, the SENSEI experiment has achieved the most stringent exclusion limit for mCPs in the 30 to 380 MeV mass range [15] using Skipper-CCDs. Based on this, additional promising scenarios for enhancing this search have been proposed using a kg-scale experiment with the same technology [16]. There is, however, a compelling reason to conduct such an experiment in the vicinity of a nuclear reactor, as its core represents the most potent source of gamma rays on Earth. Moreover, mCPs produced by Compton-like interactions from gamma rays enable the exploration of sub-MeV mass ranges, making the reactor experiments the most competitive in this energy range.

Tracking mCPs passing through a stack of detectors has also been proposed as a highly sensitive strategy for observing these particles when produced in an accelerator [17]. However, this strategy is not competitive below 1 MeV where this work is focused. In this low-mass region, values of the fraction of the elementary charge,  $\varepsilon$ , above  $10^{-4}$  have already been excluded [8]. To observe tracks for even lower values of  $\varepsilon$ , extremely large stacked detectors would be required.

In this Letter, we present world-leading direct laboratory exclusion limits for mCPs below 1 MeV, covering six orders of magnitude in mCP mass. Thus, the CONNIE and Atucha-II experiments are the first to use Skipper-CCD technology for this type of search in reactor experiments. This work also represents a collaborative effort between the two experiments, achieving combined results that enhance the robustness of the analysis and yield a stronger limit.

Approximately half of the  $\gamma$  flux in the reactor core arises from highly excited fission fragments, with the remainder originating from radioactive de-excitation of the daughter nuclei, inelastic neutron scattering, and capture of neutrons by core materials. Following [8], the  $\gamma$ -ray spectrum characteristic of neutron-induced fission of uranium, determined for an FRJ-1 (Merlin) research reactor core, can be parameterized by

$$\frac{dN_\gamma}{dE_\gamma} = K P \exp(-1.1E_\gamma), \quad (1)$$

which holds for photon energies  $E_\gamma$  above 0.2 MeV, where  $K = 0.581 \times 10^{18} \text{ MeV}^{-1} \text{ s}^{-1}$ , and  $P$  is the reactor thermal power in MW.

This model has been already employed in recent dark matter searches [2, 8, 18–20]. To the best of our knowledge, however, secondary  $\gamma$ -rays were not taken into account in previous calculations although they are also able to produce mCPs. In this work, we calculate the limits in both scenarios, reflecting the contributions to mCP production of only primary  $\gamma$ -rays, as well as including secondary  $\gamma$ -rays from transport and energy loss in the nuclear core. The secondary contribution was estimated from a simulation using GEANT4 [21, 22].

A possible channel for the generation of mCPs ( $\chi_q$ ) in the sub-GeV mass range is through a Compton-like process, in which a  $\gamma$  photon scatters off an electron in the material of the reactor core (Uranium), the photon could then kinetically mix with a dark photon [23, 24]. As a result, a new dark fermion pair  $\chi_q - \bar{\chi}_q$ , coupled to the dark photon, can acquire a small electric charge  $q = \varepsilon e$  proportional to the kinetic mixing parameter. In the case of a pure mCP, the dark photon is massless and the resulting particles has an electromagnetic charge  $\varepsilon$  which is a real number with  $|\varepsilon| < 1$  and  $e$  is the elementary charge.

The differential production cross-section for this channel can be estimated by adapting the lepton-pair production process [8]. In order to do this, the  $\chi_q - \bar{\chi}_q$  production vertex is parameterized by  $\varepsilon$  and the lepton mass is replaced by the proposed mCP mass,  $m_{\chi_q}$ ,

$$\begin{aligned} \frac{d\sigma}{dE_{\chi_q}}(\gamma e \rightarrow \chi_q \bar{\chi}_q e) &= \frac{4}{3} \frac{\varepsilon^2 \alpha^3}{m_e^2 E_\gamma^3} \times \\ &\times [(3(E_{\chi_q}^2 + E_{\bar{\chi}_q}^2) + 2E_{\chi_q} E_{\bar{\chi}_q}^2) \log\left(\frac{2E_{\chi_q} E_{\bar{\chi}_q}}{E_\gamma m_{\chi_q}}\right)], \end{aligned} \quad (2)$$

where  $m_e$  is the mass of the electron,  $\alpha$  is the fine structure constant, and  $E_{\bar{\chi}_q} = E_\gamma - E_{\chi_q}$ .

The total differential flux of millicharged particles is calculated by taking the convolution of the reactor  $\gamma$ -ray spectrum and the differential production cross-section as in Eq.3 The integral is normalized by the total interaction cross-section,  $\sigma_{\text{tot}}$ . Following the same argument

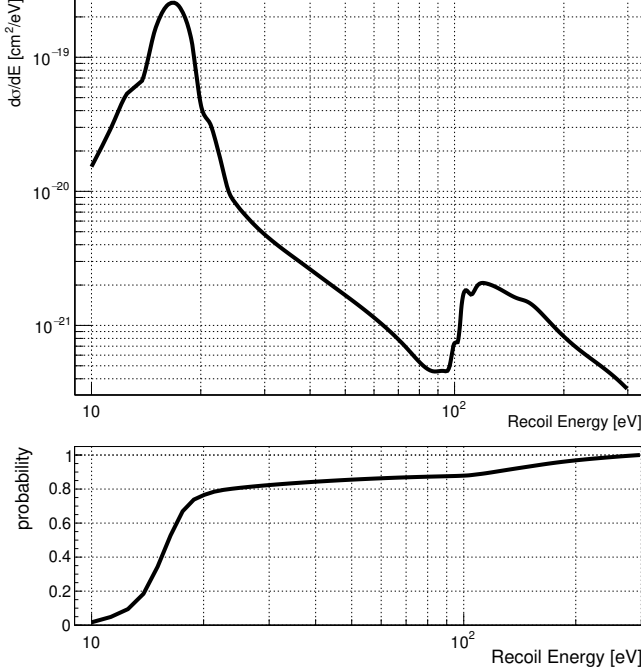


FIG. 1. (Top) Differential interaction cross-section in silicon for millicharged particles with mass  $m_{\chi_q} = 1$  eV and charge fraction  $\epsilon = 10^{-6}$ , and (bottom) cumulative probability of interaction normalized to the energy interval under consideration.

as in Refs. [8, 25],  $\sigma_{\text{tot}}$  is approximated by the Compton cross-section, restricting the integral between 1 and 5 MeV, where Compton scattering dominates over other interaction processes. The flux then becomes,

$$\frac{d\phi_{\chi_q}}{dE_{\chi_q}} = \frac{2}{4\pi D^2} \int \frac{1}{\sigma_{\text{tot}}} \frac{d\sigma}{dE_{\chi_q}} \frac{dN_\gamma}{dE_\gamma} dE_\gamma, \quad (3)$$

where  $D$  is the distance between the detector and the center of the reactor core, and there is a factor of 2 from the fact that mCPs are produced in pairs.

Millicharged particles can be described as charged particles traveling with a velocity  $\beta = \frac{p}{E_{\chi_q}}$ , and are expected to interact electromagnetically, leading to the production of ionization wherein free charge carriers are released for energy depositions above the band gap of silicon. A first description of this phenomenon can be found in Ref. [26]. This description is semiclassical in the sense that the particle is considered to be relativistic with a  $p_\mu$  and a classical source of electromagnetic fields. The effective cross-section for the interaction is then given by

$$\frac{d\sigma}{d\omega} = \frac{8\alpha\epsilon^2}{N_e\beta^2} \int_0^\infty dk \left\{ \frac{1}{k} \text{Im} \left( -\frac{1}{\epsilon(\omega, k)} \right) + k \left( \beta^2 - \frac{\omega^2}{k^2} \right) \text{Im} \left( \frac{1}{-k^2 + \epsilon(\omega, k)\omega^2} \right) \right\}, \quad (4)$$

where information regarding the interaction between virtual photons emitted by the mCP and the material is encoded in the complex dielectric function  $\epsilon(k, \omega) = \epsilon_1(k, \omega) + i\epsilon_2(k, \omega)$ ,  $N_e$  is the electron number density of the material and  $k$  is the momentum transfer to the material.

The Photo Absorption Ionization (PAI) model (also known as Fermi virtual photon or Weizsacker-Williams approximation) has been used to describe the energy loss per unit length for standard model particles, but it has also been employed in mCP searches by scaling the coupling with the electron charge to the mCP charge [27, 28]. A full derivation of the modeling of the cross-section can be found in Ref. [29], as well as a discussion on the physical meaning of each term. This differential cross-section can be expressed as

$$\frac{d\sigma}{dE} = \frac{\alpha}{\beta^2\pi} \frac{\sigma_\gamma(E)}{EZ} \ln \left[ (1 - \beta^2\epsilon_1)^2 + \beta^4\epsilon_2^2 \right]^{-1/2} + \frac{\alpha}{\beta^2\pi} \frac{1}{N_e\hbar c} \left( \beta^2 - \frac{\epsilon_1}{|\epsilon|^2} \right) \Theta + \frac{\alpha}{\beta^2\pi} \frac{\sigma_\gamma(E)}{EZ} \ln \left( \frac{2mc^2\beta^2}{E} \right) + \frac{\alpha}{\beta^2\pi} \frac{1}{E^2} \int_0^E \frac{\sigma_\gamma(E')}{Z} dE', \quad (5)$$

where  $\sigma_\gamma$  is the photoabsorption cross-section and  $\tan \Theta = \epsilon_2\beta^2/(1 - \beta^2\epsilon_1)$ .

Figure 1 illustrates the energy dependence of the interaction cross-section for an mCP with 1 eV mass and  $\epsilon = 10^{-6}$ . It is important to point out that the sizable enhancement observed in the low-energy region comes from the interaction of the particles with bulk plasmons. The tabulated complex index of refraction and photoabsorption data is not valid for energy deposits below  $\sim 50$  eV as there is a crucial difference between optical absorption and the scattering of relativistic particles. Photons are always transversely polarized, whereas a charged particle can also interact with the material via longitudinal Coulomb modes which dominate the response function in this regime. Optical absorption data have then been identified as a poor proxy for a relativistic scattering of charged particles at low energies.

To precisely calculate the interaction cross-section for mCPs near the plasmon peak, in Ref. [30] the electron loss function  $\text{Im}(-1/\epsilon(\omega, k))$  is calculated for different models of the dielectric function in the DarkELF package [31], producing reliable results when compared to electron energy loss spectroscopy data when  $\beta \geq 0.01$ . Thus, we turn to the DarkELF(GPAW) model to calculate the expected rate of mCPs below 50 eV, as PAI underestimates the cross-section near the plasmon peak, while GPAW offers a more accurate description, as stated in Ref. [30].

The differential rate of events due to  $\chi_q$  interactions can then be calculated by integrating the flux obtained in Eq. 3 convolved with the interaction cross-section,

$$\frac{dR}{dE} = \rho \int_{E_{\text{min}}}^{E_{\text{max}}} \frac{d\phi_{\chi_q}}{dE_{\chi_q}} \frac{d\sigma}{dE} dE_{\chi_q}, \quad (6)$$

where  $\rho$  is the atomic number density and ( $E_{\min}$ ,  $E_{\max}$ ) are the values of the millicharged particle energy.

Fully depleted high-resistivity silicon CCDs are being used in various experiments dedicated to dark matter [32] and low-energy neutrino detection, which require low thresholds and excellent background control. Skipper-CCDs [12] are the new generation of this imaging technology, achieving single-electron sensitivity by using the non-destructive readout of the charge packets held in each pixel [17, 33–35]. This capability allows for an excellent signal-to-noise ratio with detection thresholds as low as 15 eV in above-ground experiments [36]. Both the CONNIE and Atucha-II experiments employ Skipper-CCD sensors of 675  $\mu\text{m}$  thickness and 15  $\mu\text{m}$  pixel size, designed by LBNL Microsystems Laboratory and manufactured by Teledyne-DALSA. They are read out using a Low-Threshold Acquisition (LTA) controller board [37].

The Coherent Neutrino-Nucleus Interaction Experiment (CONNIE) [9–11, 13] is operating in a ground-level laboratory outside the dome of the 3.95 GW<sub>th</sub> Angra 2 nuclear reactor near Rio de Janeiro, Brazil, at a distance of about 30 m from the core. The experiment has been taking data with two Skipper-CCDs of 0.247 g mass each since July 2021, totaling an exposure of 18.4 g-days. The sensors achieved an ultra-low readout noise of 0.15 e<sup>-</sup> by sampling 400 times each pixel charge, allowing to measure for the first time the energy spectrum near a reactor down to a threshold of 15 eV, and obtaining a background rate in reactor-OFF data of around 4 kg<sup>-1</sup>d<sup>-1</sup>keV<sup>-1</sup> [13].

The Atucha-II nuclear power plant is a 2.175 GW<sub>th</sub> pressurized heavy water reactor that utilizes natural UO<sub>2</sub> as fuel, located in Buenos Aires province, Argentina. Since December 2021, a Skipper-CCD with 2.2 g mass is taking data inside the containment sphere, 12 m away from the nuclear core. The sensor is operated with a readout noise of 0.17 e<sup>-</sup>, achieved by averaging 300 samples of the charge in each pixel, and a background rate in reactor-OFF data of around 30 kg<sup>-1</sup>d<sup>-1</sup>keV<sup>-1</sup>. The dataset used in this work corresponds to 82 g-days of unpublished data from the 2023 run.

In the interaction cross-section from Fig. 1, the plasmon peak located between 10 and 25 eV is easily identified as the most convenient region to look for mCPs. Above 25 eV, the cross-section decreases significantly until reaching 100 eV. At this point, the energy released in the detector is sufficient to ionize the silicon *p* shell, increasing in 6 the number of electrons acting as targets. Based on this and before unblinding the data, a 200 eV energy interval starting at the lowest energy possible in each experiment was established (see Table I). It is noteworthy that the CONNIE threshold of 15 eV enables the inclusion of most of the plasmon peak while extending the interval above 240 eV for Atucha II would result in a loss of sensitivity due to the decrease in the cross-section against a constant background rate.

Table I summarizes the results obtained from each ex-

perimental run. Upper limits at 90% C.L. on the numbers of events were computed using the frequentist approach, as outlined in Ref. [38]. Efficiency corrections were implemented by convolving the expected theoretical event count with the efficiency curves from Refs. [13, 14].

Figure 2 depicts the resulting independent exclusion limits attained by each experiment. The solid lines show the main results, based on limits obtained from including both the primary and the secondary  $\gamma$ -ray contributions to mCP production. For comparison with the previous limit by the TEXONO collaboration [8], the exclusion limits were also calculated based on mCP production from only primary  $\gamma$ -rays (dashed lines). The results show an improvement by both the CONNIE and Atucha-II experiments, for both cases of primary and secondary, or only primary  $\gamma$ -ray production. Moreover, a combined analysis of the outcomes from both experiments is performed following Ref. [38], yielding a further improvement on the individual results (see Supplemental Material [39] for details).

The mCP search is particularly challenging because the number of observed events scales with  $\varepsilon^4$ . A factor  $\varepsilon^2$  originates from the mCP production within the reactor core (Eq. 3), while another factor  $\varepsilon^2$  results from the probability of interaction (Eq. 4). Therefore, achieving an improvement in the limit by an order of magnitude requires increasing either the experimental exposure or the mCP flux by a factor of 10<sup>4</sup>. The former is experimentally highly demanding, and the latter is almost impossible for accelerator experiments. In the case of reactor experiments, the flux scales linearly with the power but inversely with the square of the distance. Achieving such an increment in flux would entail reducing the distance by a factor of a hundred, which is impractical for most cases. On the other hand, systematic uncertainties are mitigated by the fourth power dependence on the expected number of events. The main contribution stems from the matching of DarkELF(GPAW) and PAI cross-sections at 50 eV, introducing a 50% systematic uncertainty. This uncertainty translates into a 10% uncertainty in the exclusion limits.

We have demonstrated an alternative approach to improving limits by reducing the detection threshold to exploit the significant enhancement in the cross-section. Skipper-CCD technology, which combines the 1.1 eV sil-

TABLE I. Experimental observables of each experiment.

Observable	CONNIE	Atucha-II
Reactor ON exposure [g-day]	14.9	59.4
Reactor OFF exposure [g-day]	3.5	22.6
Energy bin [eV]	15–215	40–240
Reactor ON counts	6	168
Reactor OFF counts	2	71
90% C.L. upper limit on events	6.2	30.9

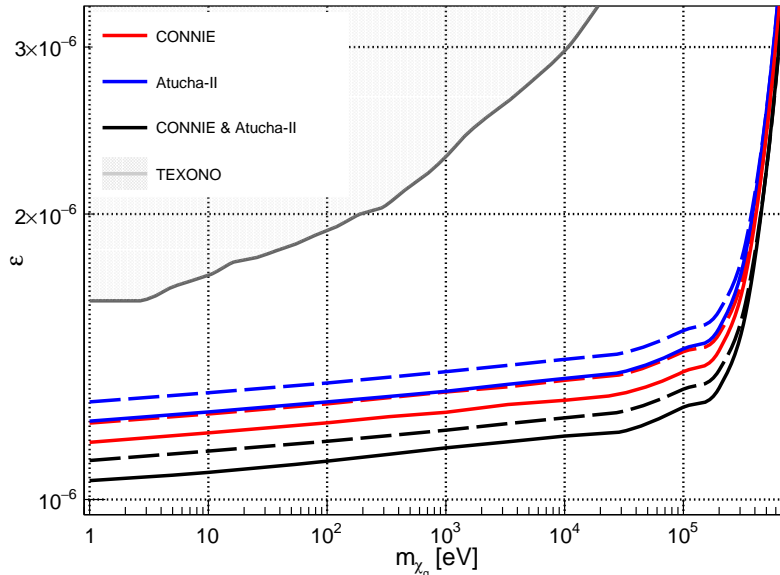


FIG. 2. Exclusion limits at 90% C.L. as a function of the mCP mass and charge fraction for CONNIE (red), Atucha-II (blue) and the combination of the two experiments (black). Solid lines correspond to results obtained when considering mCP production from both primary and secondary  $\gamma$ -rays, while dashed lines account for only primary  $\gamma$ -rays. The TEXONO exclusion limit [8] is also included for comparison.

icon band gap with sub-electron readout noise, enables experiments with sensitivity at the eV scale, presenting a unique opportunity. The capability of observing interactions at the eV scale allows CONNIE to take advantage of the plasmon resonance [40]. This collective mode of electronic excitation in semiconductor materials significantly enhances the detection sensitivity for sub-MeV relativistic particles. Accessing recoil energies in the eV range results in a flatter cross-section dependence on mCP mass, compared to the TEXONO experiment, which operated above 300 eV, showing a logarithmic dependence on the inverse of the mCP mass through the equivalent photon approximation cross-section [8]. The Atucha-II experiment possesses a three times higher mCP flux and a four times higher reactor ON exposure compared to the CONNIE experiment. This is compensated by the fact that the CONNIE's energy interval accounts for a 4.5 times larger probability of mCP interaction (see Fig. 1) than Atucha's energy interval, as well as a background rate six times lower. Consequently, both experiments feature a similar signal-to-square-root-of-background ratio, which explains the closeness of the achieved exclusion limits.

We also present for the first time a combined analysis of the collaborative effort between the two experiments, resulting in a very robust limit that strongly mitigates systematic errors eventually introduced by any of them. The combined result extends the experimental exclusion limits further towards 720 keV in mCP mass, as well as down towards  $\epsilon \sim 1 \times 10^{-6}$  for the lowest mCP masses of

1 eV, thus becoming the best direct laboratory constraint on mCP coupling. It is noteworthy that both reactor experiments are currently conducting this search with only around 1g of sensor, and both projects have plans for substantial increases in sensor mass [13, 14, 41, 42].

CONNIE thanks the Silicon Detector Facility staff at the Fermi National Accelerator Laboratory for hosting the assembly and test of the detector components used in the CONNIE experiment. The CCD development was partly supported by the Office of Science, of the U.S. Department of Energy under Contract No. DE-AC02-05CH11231. We are grateful to Eletrobras Eletronuclear, and especially to G. Coelho, I. Soares, I. Ottoni and L. Werneck, for access to the Angra 2 reactor site, infrastructure and the support of their personnel. We express gratitude to R. Sheldard (in memoriam) for supporting the experiment. We thank M. Giovani for the IT support and M. Martínez Montero for the technical assistance. We acknowledge the support from the Brazilian Ministry for Science, Technology, and Innovation and the funding agencies FAPERJ, CNPq and FINEP; Argentina's CONICET and AGENCIA I+D+i; (grants PICT-2019-2019-04173; PICT-2021-GRF-TII-00458; PICT-2021-GRF-TI-00816) and the LAA-HECAP Network. We acknowledge the support from Mexico's CONAHCYT (grant CF-2023-I-1169) and DGAPA-UNAM (PAPIIT grant IN104723). This work made use of the CHE cluster, managed and funded by COSMO/CBPF/MCTI, with financial sup-

port from FINEP and FAPERJ, and operating at the Javier Magnin Computing Center/CBPF.

Atucha-II thanks the NA-SA team in Argentina for all the support during the deployment and operation of the Skipper-CCD system at Atucha-II. This work was supported by Fermilab under DOE Contract No. DE-AC02-07CH11359. We thank Eneas Kapou from NA-SA for assisting in data transportation outside the plant. We thank Daniel Cartelli from CNEA for creating the artistic plots of the plant and the system. We also want to thank Eduardo Arostegui who insisted on carrying on with the project and facilitated a lot the communication with the plant during the first phase of the deployment.

---

\* santiep.137@gmail.com

† rodriguesfm@df.uba.ar

- [1] J. B. Dent, B. Dutta, D. Kim, S. Liao, R. Mahapatra, K. Sinha, and A. Thompson, New Directions for Axion Searches via Scattering at Reactor Neutrino Experiments, *Phys. Rev. Lett.* **124**, 211804 (2020), arXiv:1912.05733 [hep-ph].
- [2] D. Aristizabal Sierra, V. De Romeri, L. J. Flores, and D. K. Papoulias, Axionlike particles searches in reactor experiments, *JHEP* **03**, 294, arXiv:2010.15712 [hep-ph].
- [3] Z. Atif *et al.* (RENO, NEOS), Search for sterile neutrino oscillations using RENO and NEOS data, *Phys. Rev. D* **105**, L111101 (2022), arXiv:2011.00896 [hep-ex].
- [4] M. Andriamirado *et al.* (PROSPECT, (PROSPECT Collaboration)\*), Limits on sub-GeV dark matter from the PROSPECT reactor antineutrino experiment, *Phys. Rev. D* **104**, 012009 (2021), arXiv:2104.11219 [hep-ex].
- [5] M. Andriamirado *et al.* (PROSPECT), PROSPECT-II physics opportunities, *J. Phys. G* **49**, 070501 (2022), arXiv:2107.03934 [hep-ex].
- [6] M. I. Dobroliubov and A. Y. Ignatiev, MILLICHARGED PARTICLES, *Phys. Rev. Lett.* **65**, 679 (1990).
- [7] G. Magill, R. Plestid, M. Pospelov, and Y.-D. Tsai, Millicharged particles in neutrino experiments, *Phys. Rev. Lett.* **122**, 071801 (2019), arXiv:1806.03310 [hep-ph].
- [8] L. Singh *et al.* (TEXONO), Constraints on millicharged particles with low threshold germanium detectors at Kuo-Sheng Reactor Neutrino Laboratory, *Phys. Rev. D* **99**, 032009 (2019), arXiv:1808.02719 [hep-ph].
- [9] A. Aguilar-Arevalo *et al.* (CONNIE), Exploring low-energy neutrino physics with the Coherent Neutrino Nucleus Interaction Experiment, *Phys. Rev. D* **100**, 092005 (2019), arXiv:1906.02200 [physics.ins-det].
- [10] A. Aguilar-Arevalo *et al.* (CONNIE), Search for coherent elastic neutrino-nucleus scattering at a nuclear reactor with CONNIE 2019 data, *JHEP* **05**, 017, arXiv:2110.13033 [hep-ex].
- [11] A. Aguilar-Arevalo *et al.* (CONNIE), Search for light mediators in the low-energy data of the CONNIE reactor neutrino experiment, *JHEP* **04**, 054, arXiv:1910.04951 [hep-ex].
- [12] J. Tiffenberg, M. Sofo-Haro, A. Drlica-Wagner, R. Essig, Y. Guardincerri, S. Holland, T. Volansky, and T.-T. Yu (SENSEI), Single-electron and single-photon sensitivity with a silicon Skipper CCD, *Phys. Rev. Lett.* **119**, 131802 (2017), arXiv:1706.00028 [physics.ins-det].
- [13] A. A. Aguilar-Arevalo *et al.* (CONNIE), Searches for CE $\nu$ NS and Physics beyond the Standard Model using Skipper-CCDs at CONNIE, (2024), arXiv:2403.15976 [hep-ex].
- [14] E. Depaoli *et al.*, Deployment and performance of a low-energy-threshold skipper-ccd inside a nuclear reactor, (2024), arXiv:2401.07885 [hep-ex].
- [15] L. Barak *et al.* (SENSEI), SENSEI: Search for Millicharged Particles produced in the NuMI Beam, (2023), arXiv:2305.04964 [hep-ex].
- [16] A. Aguilar-Arevalo *et al.* (Oscura), The Oscura Experiment, (2022), arXiv:2202.10518 [astro-ph.IM].
- [17] S. Perez *et al.* (Oscura), Searching for millicharged particles with 1 kg of Skipper-CCDs using the NuMI beam at Fermilab, *JHEP* **02**, 072, arXiv:2304.08625 [hep-ex].
- [18] H. Park, Detecting Dark Photons with Reactor Neutrino Experiments, *Phys. Rev. Lett.* **119**, 081801 (2017), arXiv:1705.02470 [hep-ph].
- [19] F. Arias-Aragón, V. Brdar, and J. Quevillon, New Directions for ALP Searches Combining Nuclear Reactors and Haloscopes, (2023), arXiv:2310.03631 [hep-ph].
- [20] M. Smirnov, G. Yang, J. Liao, Z. Hu, and J. Ling, Light dark bosons in the JUNO-TAO neutrino detector, *Phys. Rev. D* **104**, 116024 (2021), arXiv:2109.04276 [hep-ex].
- [21] S. Agostinelli *et al.* (Geant4 collaboration), Geant4: A simulation toolkit, *Nucl. Instrum. Meth.* **A506**, 250 (2003).
- [22] J. Allison, K. Amako, J. Apostolakis, H. Araujo, P. Dubois, *et al.* (Geant4 collaboration), Geant4 developments and applications, *IEEE Trans.Nucl.Sci.* **53**, 270 (2006).
- [23] P. Adshead, P. Ralegankar, and J. Shelton, Dark radiation constraints on portal interactions with hidden sectors, *JCAP* **09**, 056, arXiv:2206.13530 [hep-ph].
- [24] W.-Z. Feng, Z.-H. Zhang, and K.-Y. Zhang, Sub-GeV millicharge dark matter from the  $U(1)_X$  hidden sector, (2023), arXiv:2312.03837 [hep-ph].
- [25] S. N. Gninenko, N. V. Krasnikov, and A. Rubbia, New limit on millicharged particles from reactor neutrino experiments and the p $\nu$ ls anomaly, *Phys. Rev. D* **75**, 075014 (2007).
- [26] E. Fermi, The ionization loss of energy in gases and in condensed materials, *Phys. Rev.* **57**, 485 (1940).
- [27] I. Alkhatib *et al.* (SuperCDMS), Constraints on Lightly Ionizing Particles from CDMSlite, *Phys. Rev. Lett.* **127**, 081802 (2021), arXiv:2011.09183 [hep-ex].
- [28] K. Kamdin, *Search for Lightly Ionizing Particles in the LUX Detector and Research and Development For Future Liquid Xenon Time Projection Chambers* (University of California, Berkeley, 2018).
- [29] W. W. M. Allison and J. H. Cobb, Relativistic Charged Particle Identification by Energy Loss, *Ann. Rev. Nucl. Part. Sci.* **30**, 253 (1980).
- [30] R. Essig, R. Plestid, and A. Singal, Collective excitations and low-energy ionization signatures of relativistic particles in silicon detectors, (2024), arXiv:2403.00123 [hep-ph].
- [31] S. Knapen, J. Kozaczuk, and T. Lin, python package for dark matter scattering in dielectric targets, *Phys. Rev. D* **105**, 015014 (2022).
- [32] A. Aguilar-Arevalo *et al.* (DAMIC), Results on low-mass weakly interacting massive particles from a 11 kg-day target exposure of DAMIC at SNOLAB, *Phys. Rev. Lett.*

- 125**, 241803 (2020), arXiv:2007.15622 [astro-ph.CO].
- [33] I. Arnquist, N. Avalos, D. Baxter, X. Bertou, N. Castelló-Mor, A. Chavarria, J. Cuevas-Zepeda, J. C. Gutiérrez, J. Duarte-Campderros, A. Dastgheibi-Fard, O. Deligny, C. De Dominicis, E. Estrada, N. Gadola, R. Gaïor, T. Hossbach, L. Iddir, L. Khalil, B. Kilminster, A. Lantero-Barreda, I. Lawson, S. Lee, A. Letessier-Selvon, P. Loaiza, A. Lopez-Virto, A. Matalon, S. Munagavalasa, K. McGuire, P. Mitra, D. Norcini, G. Papadopoulos, S. Paul, A. Piers, P. Privitera, K. Ramanathan, P. Robmann, M. Settimo, R. Smida, R. Thomas, M. Traina, I. Vila, R. Vilar, G. Warot, R. Yajur, and J.-P. Zopounidis, First constraints from DAMIC on sub-gev dark-matter particles interacting with electrons, *Physical Review Letters* **130**, 10.1103/physrevlett.130.171003 (2023).
- [34] A. Aguilar-Arevalo *et al.* (SENSEI, DAMIC-M, DAMIC), Confirmation of the spectral excess in DAMIC at SNOLAB with skipper CCDs, *Phys. Rev. D* **109**, 062007 (2024), arXiv:2306.01717 [astro-ph.CO].
- [35] P. Adari *et al.* (SENSEI), SENSEI: First Direct-Detection Results on sub-GeV Dark Matter from SENSEI at SNOLAB, (2023), arXiv:2312.13342 [astro-ph.CO].
- [36] G. F. Moroni, F. Chierchie, J. Tiffenberg, A. Botti, M. Cababie, G. Cancelo, E. L. Depaoli, J. Estrada, S. E. Holland, D. Rodrigues, I. Sidelnik, M. S. Haro, L. Stefanazzi, and S. Uemura, Skipper charge-coupled device for low-energy-threshold particle experiments above ground, *Phys. Rev. Appl.* **17**, 044050 (2022).
- [37] G. I. Cancelo *et al.*, Low Threshold Acquisition controller for Skipper CCDs, *J. Astron. Telesc. Instrum. Syst.* **7**, 015001 (2021), arXiv:2004.07599 [astro-ph.IM].
- [38] G. Cowan, K. Cranmer, E. Gross, and O. Vitells, Asymptotic formulae for likelihood-based tests of new physics, *Eur. Phys. J. C* **71**, 1554 (2011), [Erratum: *Eur. Phys. J. C* **73**, 2501 (2013)], arXiv:1007.1727 [physics.data-an].
- [39] See Supplemental Material at URL-will-be-inserted-by-publisher for the statistical formalism applied for obtaining the limits.
- [40] Z.-L. Liang, L. Su, L. Wu, and B. Zhu, Plasmon-enhanced Direct Detection of sub-MeV Dark Matter, (2024), arXiv:2401.11971 [hep-ph].
- [41] G. Fernandez Moroni, P. Machado, I. Martinez-Soler, Y. Perez-Gonzalez, D. Rodrigues, and S. Rosauro-Alcaraz, The physics potential of a reactor neutrino experiment with skipper ccds: measuring the weak mixing angle, *Journal of High Energy Physics* **2021** (2021).
- [42] G. Fernandez-Moroni, R. Harnik, P. A. N. Machado, I. Martinez-Soler, Y. F. Perez-Gonzalez, D. Rodrigues, and S. Rosauro-Alcaraz, The physics potential of a reactor neutrino experiment with skipper-ccds: searching for new physics with light mediators, *Journal of High Energy Physics* **127** (2022).

## SUPPLEMENTAL MATERIAL

### Nuclear reactor $\gamma$ -ray spectrum

The photon flux and photon spectrum typically used in the calculation for the production of new particle candi-

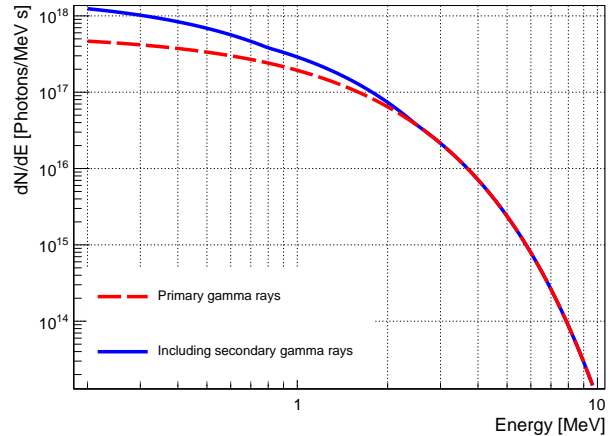


FIG. 3. Photon flux produced in the nuclear reactor. The red dashed line is derived from Eq. 1, considering primary  $\gamma$ -rays only. The blue solid line is obtained from a GEANT4 simulation, taking into account secondary photon production.

dates are approximations of the fission prompt  $\gamma$ -rays or delayed  $\gamma$ -rays from fission products. For example, the spectrum produced in Eq. 1 is the photon production resulting from neutron capture in  $^{235}\text{U}$ . Most analyses do not consider the transport and energy loss of these photons in the reactor core as an additional production probability for generating the particles of interest. Since the photons lose energy due to the successive scattering, this additional probability of production of exotic particles will favor those with lower energy.

A simulation was performed using GEANT4 [21, 22] to transport primary photons produced in the core. A single-volume geometry of the uranium element was used to track the successive interactions of  $\gamma$  particles. The particle source of  $\gamma$ -rays follows Eq. 1 generated isotropically in the center of the volume. The interactions of the  $\gamma$ -rays are tracked through the volume, with the energy before each interaction recorded as a candidate for interactions in the material core. Figure 3 shows the original primary  $\gamma$  spectrum and the one including secondary photons from the simulation of interacting prompt photons. The additional secondary photons are more prominent in the low-energy part of the spectrum.

### Statistical formalism

To obtain the upper limit of  $\varepsilon$ , we followed the approach of Ref. [38], based on computing the likelihood profile ratio. The two measured random variables in our experiments are the detected number of events in a given energy interval for the reactor-ON ( $n$ ) and reactor-OFF ( $m$ ) runs. Thus, the likelihood function of each experiment can be expressed as the product of the reactor-ON



and the reactor-OFF Poisson distributions:

$$L(\mu, b) = \frac{(\mu s + b)^n}{n!} e^{-(\mu s + b)} \times \frac{(\tau b)^m}{m!} e^{-(\tau b)} ,$$

where  $\mu$  denotes the strength parameter,  $s$  is the expected number of counts for a given charge fraction  $\varepsilon_0$  in that energy interval (given by the theoretical prediction),  $b$  is the mean number of expected background events in the reactor-ON data, and  $\tau$  is a factor that corrects  $b$  to the exposure of reactor OFF:  $\tau = \frac{\text{exposure OFF}}{\text{exposure ON}}$ .

To determine the upper limit of  $\mu$ , we first compute the profile likelihood ratio and then the statistic  $t_\mu$ :

$$\lambda \equiv \frac{L(\mu, \hat{b})}{L(\hat{\mu}, \hat{b})} \quad \text{and} \quad t_\mu \equiv -2 \ln(\lambda) .$$

Here  $\hat{\mu}$  and  $\hat{b}$  are the maximum likelihood estimators and  $\hat{b}$  is the result of maximizing the parameter  $b$  for a given value of  $\mu$ . Usually,  $b$  is called a *nuisance parameter*. The statistic  $t_\mu$  has a chi-squared probability distribution with 1 degree of freedom ( $f(t_\mu|\mu)$ ). This can be used to compute the p-value of the particular experimental realization for a given hypothesis  $\mu$ :

$$\text{p-value} = \int_{t_{\mu, \text{obs}}}^{\infty} f(t_\mu|\mu) dt_\mu .$$

The upper limit of  $\mu$  with a  $\alpha\%$  confidence level corresponds to the value of this parameter that gives a p-value =  $1 - \alpha$ . Then, the upper limit of  $\varepsilon$  is calculated as  $\sqrt[4]{\mu} \varepsilon_0$ .

This procedure can be applied for each experiment separately but also represents a useful and robust framework for obtaining the upper limit of a combination of the two experiments. In this case, the total experiment has four measured random variables ( $n_a, m_a, n_c, m_c$ ) where the  $a$  and  $c$  indices correspond to Atucha-II and CONNIE, respectively. Since the two experiments are independent, the new combined likelihood is the product of the two single likelihoods:

$$\prod_{i=a,c} \frac{L(\mu, b_a, b_c)}{L(\hat{\mu}, \hat{b}_a, \hat{b}_c)} = \prod_{i=a,c} \frac{(\mu s_i + b_i)^{n_i}}{n_i!} e^{-(\mu s_i + b_i)} \times \frac{(\tau b_i)^{m_i}}{m_i!} e^{-(\tau b_i)} .$$

Here all  $b_i$  are nuisance parameters. The likelihood profile ratio translates into  $\lambda = \frac{L(\mu, \hat{b}_a, \hat{b}_c)}{L(\hat{\mu}, \hat{b}_a, \hat{b}_c)}$ . The expected number of events  $s_i$  has to be calculated for each experiment because the energy intervals could differ, but the rest of the procedure remains the same. The combination of the two experiments shows a more restricted  $\alpha$  confidence level interval since it incorporates both realizations as evidence of the absence of millicharged particles.